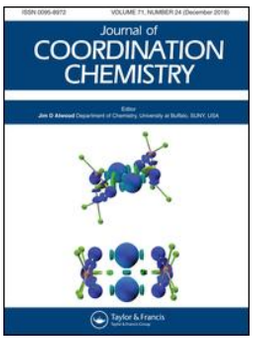

Taylor & Francis
Taylor & Francis Group

Journal of Coordination Chemistry

ISSN: 0095-8972 (Print) 1029-0389 (Online) Journal homepage: https://www.tandfonline.com/loi/gcoo20

# Syntheses, structure, DNA-binding and DFT studies of a Cu(II) complex based on a pyrazolone derivative

Wei Xi, Cai-Yun Wang, Huan-Huan Meng & Xue-Qin Song

**To cite this article:** Wei Xi, Cai-Yun Wang, Huan-Huan Meng & Xue-Qin Song (2019): Syntheses, structure, DNA-binding and DFT studies of a Cu(II) complex based on a pyrazolone derivative, Journal of Coordination Chemistry, DOI: 10.1080/00958972.2019.1680835

**To link to this article:** https://doi.org/10.1080/00958972.2019.1680835

JOURNAL OF COORDINATION CHEMISTRY
https://doi.org/10.1080/00958972.2019.1680835

Taylor & Francis
Taylor & Francis Group



# Syntheses, structure, DNA-binding and DFT studies of a Cu(II) complex based on a pyrazolone derivative

Wei Xi, Cai-Yun Wang, Huan-Huan Meng and Xue-Qin Song

School of Chemical and Biological Engineering, Lanzhou Jiaotong University, Lanzhou, China

**ABSTRACT**

A Cu(II) complex based on a pyrazolone derivative, 2-hydroxy-N′-((1-(4-methoxyphenyl)-3methyl-5-oxo-4,5-dihydro-1H-pyrazol-4-yl)(phenyl)methylene)benzohydrazide ($H_2L$), has been prepared. IR spectra, UV-vis spectra, elemental analysis and single-crystal X-ray diffraction indicate that the Cu(II) complex was mononuclear with the chemical composition of $[Cu(HL)Cl]\cdot CH_3OH$. The Cu(II) compound presented herein exhibits interesting supramolecular characteristics and a novel 3D supramolecular architecture resulted due to the appropriate synergy of multiple intermolecular hydrogen bonds. The interaction of the Cu(II) complex with calf-thymus DNA was investigated by electronic absorption titration as well as EB-DNA competition experiment, and the results indicate that the Cu(II) compound which has a strong affinity for binding DNA is combined with DNA in an embedded manner. Furthermore, Time-Dependent Density Functional Theory calculations (TD-DFT) have been performed on optimized geometries for a better understanding of the electronic transitions in the UV-vis spectra of $H_2L$ and Cu(II) complex.

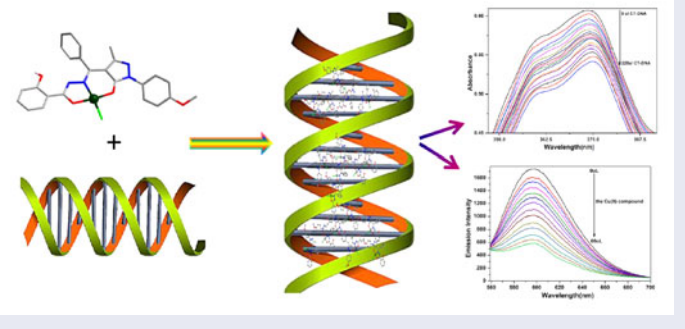

**ARTICLE HISTORY**
Received 1 August 2019
Accepted 23 September 2019

**KEYWORDS**
Pyrazolone; Cu(II) compound; crystal structure; DNA binding; DFT calculations

## 1. Introduction

Cancer is a major chronic disease that seriously endangers human health and it is documented that many cancers, such as lung cancer, skin cancer or breast cancer,

**CONTACT** Xue-Qin Song songxq@mail.lzjtu.cn School of Chemical and Biological Engineering, Lanzhou Jiaotong University, Lanzhou 730070, China

Supplemental data for this article is available online at https://doi.org/10.1080/00958972.2019.1680835.

have been found to have different symptoms and causes, but all are caused by abnormalities in DNA sequences [1]. Meanwhile, numerous biological experiments have demonstrated that DNA is the main target for anticancer drugs [2, 3]. For example, the mechanism of carboplatin for treating cancer is that it mainly crosslinked with the DNA chain of cells to destroy DNA and inhibit tumor growth [4]. Therefore, studies on the interaction of compounds with DNA is attracting attention and as a result, huge quantities of such compounds, including metal compounds have been reported [5, 6]. For instance, Pt(II) complex displays an efficient DNA-binding ability in an intercalative mode and certain Pt(II) complexes could efficiently cleave DNA with a micromolar concentration without any external reagents [7, 8]. In addition, the Mn(II), Pd(II), and Co(II) complexes all could bind calf-thymus DNA (CT-DNA) *via* intercalation in-between DNA-bases [9–12]. The action effect of Cu(II) complex on DNA have been studied for developing novel anticancer drugs [13]since the mixture of copper chloride and lecithin was utilized to treat facial cancer patients in Germany in 1912. As one of the indispensable trace elements in the human body, copper plays important roles in life activities, such as energy metabolism, respiration and DNA synthesis. Copper exists in all organs and tissues of people, and is usually in combination with proteins or other organic compounds, rather than as free copper ions [14, 15]. Copper has the effect of cracking nucleic acids directly due to its variable coordination structure and catalytic activity of activated small molecules [16], which renders it special biological activity and catalytic effect on the life system.

4-Acylpyrazolone is a kind of heterocyclic β-diketone type chelating agent, which can form a large number of complexes with various metal ions due to its multiple potential chelating sites including oxygen and nitrogen atoms. In addition, pyrazolone compounds have a variety of biological activities, including anti-inflammatory, antibacterial, and antitumor [17, 18], which makes them hot spots in the field for developing new antitumor drugs [19]. Therefore, it is of great significance to develop new pyrazolone compounds and apply them to prepare coordination compounds for the development of metal antitumor drugs.

Based on the above consideration and extend our study on coordination chemistry of pyrazolone derivatives [20], a new pyrazolone derivative, 2-hydroxy-N′-((1-(4-methoxyphenyl)3-methyl-5-oxo-4,5-dihydro-1H-pyrazol-4-yl)(phenyl)methylene)benzohydrazide ($H_2L$), was prepared to construct new coordination compounds for biological activity study. The salicylyl group was introduced in $H_2L$ herein to obtain more stable metal compounds due to the increased chelating sites. Hence, a Cu(II) compound was afforded and well characterized by IR spectra, UV-vis spectra, elemental analysis and X-ray diffraction. The DNA-binding effect of the $H_2L$ and Cu(II) complex was studied by UV-vis and fluorescence spectra. In addition, Time-Dependent Density Functional Theory calculations (TD-DFT) have been performed on optimized geometries for a better understanding of the electronic transitions in the UV-vis spectra of $H_2L$ and Cu(II) complex.

## 2. Materials and methods

### *2.1. Materials and physical measurements*

P-methoxyphenyl hydrazine hydrochloride, ethyl acetoacetate, glacial acetic acid, methyl salicylate, hydrazine hydrate (80%), NaOH, $NH_4Cl$, methanol and ethanol were

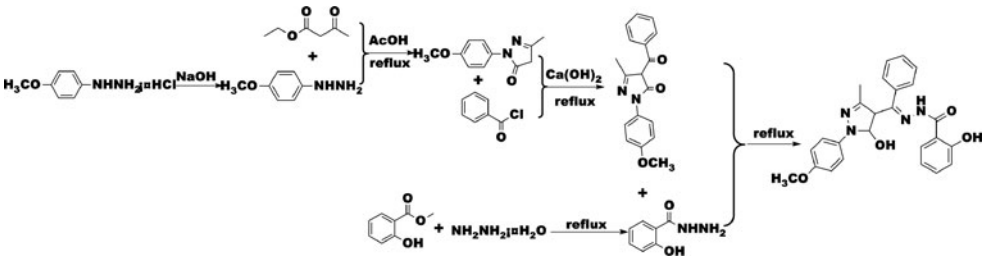

Scheme 1. The synthetic route of $H_2L$.

from commercial sources and not further purified. All chemicals were analytical grade. 4-Benzoyl-2-(4-methoxy-phenyl)-5-methyl-2,4-dihydro-pyrazol-3-one and salicylhydrazide were prepared according to the literature [21]. CT-DNA was purchased from Yuanye Biotechnology Company (Shanghai, China). The UV absorption ratio of CT-DNA solution at 260 and 280 nm was about 1.8 ~ 1.9, indicating that CT-DNA contained no protein [22]. The CT-DNA concentration of each nucleotide was determined by spectrophotometry using the extinction coefficient of 6600 $cm^{-1}$ at 260 nm [23].

Carbon, nitrogen, and hydrogen analyses were performed using an EL elemental analyzer. Infrared spectra were obtained with KBr discs on a Thermo Mattson FTIR spectrometer from 4000 ~ 400 $cm^{-1}$ with an average of 128 scans and 4 $cm^{-1}$ of spectral resolution. UV-vis absorption spectra were determined with a UV-1800 Shimadzu spectrophotometer. Emission fluorescence spectra were recorded on an F-7000 fluorescence spectrophotometer (Japan Hitachi company) at room temperature. The width of the excitation and emission slits are both 5.0 nm. $^1H$ and $^{13}C$ NMR spectra were recorded in $CDCl_3$ solution at room temperature on a Bruker 500 instrument operating at a frequency of 500 MHz and referenced to tetramethylsilane (0.00 ppm) as an internal standard.

## 2.2. Synthesis of the ligand

The synthetic route for $H_2L$ is shown in Scheme 1. To an ethanolic solution (10 mL) containing 2.28 g (3 mmol) 4-benzoyl-2-(4-methoxy-phenyl)-5-methyl-2,4-dihydro-pyrazol-3-one, an ethanolic solution of 0.46 g (3 mmol) salicylhydrazide and 0.5 mL acetic acid was added dropwise within 30 min. The reaction mixture was continuously stirred and refluxed at 80 °C for 4 h. After the resulted solution was cooled to room temperature, 10 mL water were added and the mixture was further stirred to obtain precipitates which was filtered and recrystallized from ethanol to afford yellow solids. $H_2L$: 0.93 g, Yield: 70%. $^1H$ NMR ($CDCl_3$, 500 MHz), $\delta$ (ppm): 1.54 (s, 3H), 3.78 (s, 1H), 3.84 (s, 3H), 6.97 (dd, 4H), 7.47 (m, 1H), 7.68 (m, 6H), 7.84 (t, 3H), 11.70(s, 1H). $^{13}C$ NMR ($CDCl_3$, 400 MHz), $\delta$ (ppm): 166.61, 157.50, 149.04, 135.00, 132.69, 129.75, 129.46, 129.07, 127.45, 122.43, 119.55, 118.22, 114.06, 113.96, 55.52, 55.45, 16.11. Anal. Calcd for $C_{25}H_{22}N_4O_4$: C, 67.86; H, 5.01; N, 12.66. Found: C, 66.69; H, 5.04; N, 12.62.

## 2.3. Synthesis of the Cu(II) complex

Seventeen milligrams of (0.1 mmol) $CuCl_2 \cdot 2H_2O$ in 4 mL methanol was added dropwise to a 2 mL methanol solution of 44 mg (0.1 mmol) $H_2L$ at room temperature, and the

**Table 1.** Crystallographic data and data collection parameters for the Cu(II) complex.

| | |
|---|---|
| Empirical formula | $CuC_{26}H_{25}ClN_4O_5$ |
| Temperature (K), M | 296(2), 572.5 |
| Crystal system, Space group | Monoclinic, $P2_1/c$ |
| Unit cell dimensions | $a$ = 9.8688(12) Å, $\alpha$= 90.00° $b$ = 15.217(3) Å, $\beta$=103.072(3)° $c$ = 18.178(2) Å, $\gamma$ = 90.00° |
| Volume (Å$^3$), $Z$ | 2667.8(6), 4 |
| Absorption coefficient (mm$^{-1}$) | 0.962 |
| $F$(000) | 1180 |
| $\theta$ Range for data collection (°) | 3.45 ~ 25.00 |
| Index ranges | $-11 \leq h \leq 11$; $-18 \leq k \leq 16$; $-21 \leq l \leq 19$ |
| Reflections collected/unique | 13211/4684 |
| $R_{int}$ | 0.0289 |
| Data / restraints / parameters | 4784 / 1 / 343 |
| Goodness-of-fit on $F^2$ | 1.029 |
| Final $R$ indices [$I > 2\sigma(I)$] | $R_1$ = 0.0441, $wR_2$ = 0.1260 |
| $R$ indices (all data) | $R_1$ = 0.0594, $wR_2$ = 0.1398 |

reaction mixture was stirred subsequently for 4 h at room temperature to obtain a large amount of precipitate. Then, 30 mL methanol were added to dissolve the precipitation, and the resulted solution was filtered into several 10-mL glass vials for evaporation. Single-crystals suitable for crystal analysis were obtained after three weeks when solvent was partially evaporated. Yield: 24 mg, 42% based on $H_2L$. Anal. Calcd for $CuClC_{26}H_{25}N_4O_5$: C, 54.55; H, 4.40; 9.79. Found: C, 54.74; H, 4.38; N, 9.75.

### 2.4. X-ray single-crystal diffraction analysis

Single-crystal X-ray diffraction data were recorded on an Oxford Diffraction Gemini R Ultra diffractometer with graphite-monochromated Mo Kα radiation ($\lambda$ = 0.71073 Å) at 293 K. Absorption corrections were applied using a multi-scan technique. No crystal decay was noted during the data collections. The frames were integrated with the Bruker SAINT software package using a narrow-frame algorithm. Data were corrected for absorption effects using the empirical multi-scan method (SADABS) [24]. The structures were solved by direct methods and refined on $F^2$ by a full-matrix least-squares procedure. SHELXL-2014 was used for both structural solutions and refinements [25]. Non-hydrogen atoms of the compounds were refined with anisotropic temperature parameters. All hydrogens were placed in geometrically idealized positions (C–H = 0.96 Å for methyl groups, C–H = 0.97 Å for $CH_2$ groups, C–H = 0.93 Å for phenyl groups and O–H = 0.82 Å for hydroxyl groups) and constrained to ride on their parent atoms with $U_{iso}$ (H) = 1.5 $U_{eq}$(C) for methyl groups, 1.2 $U_{eq}$(C) for aromatic and $CH_2$ groups, and 1.5 $U_{eq}$(O) for hydroxyl groups. The crystal structure parameters of the Cu(II) complex are given in Table 1. Graphics were drawn with DIAMOND (Version 3.2) [26].

## 3. Results and discussion

### 3.1. Synthesis and characterization

$H_2L$ was prepared as yellow solid in four steps from the commercially available p-methoxyphenyl hydrazine hydrochloride, methyl salicylate and hydrazine hydrate as

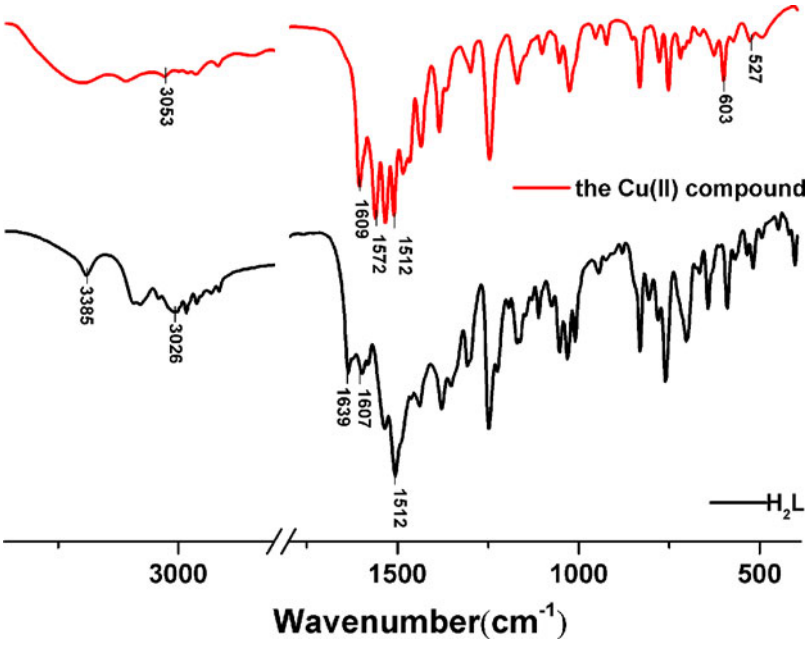


**Figure 1.** IR spectra of $H_2L$ and Cu(II) complex in solid state.

shown in Scheme 1. The $^1H$ and $^{13}C$ NMR spectra (Supplementary material, Figures S1 and S2) confirmed the identity of $H_2L$. The formation of Cu(II) complex was first ascertained by the IR spectra determination. As shown in Figure 1, a wide characteristic absorption band at 3385 $cm^{-1}$ characteristic of enolic group on pyrazolone and the absence of band from ketone carbonyl ascertained that $H_2L$ exists in the form of enolic in the solid. The band at 3025 $cm^{-1}$ is assigned to the phenolic hydroxyl group of ligand. The strong band at 1639 $cm^{-1}$ from the stretching vibrations of the acylhydrazone C = O with the acylhydrazone C = N and the pyrazole ring C = N stretching vibrations appeared at 1607 and 1512 $cm^{-1}$, respectively. By contrast, in the IR spectra of the complex $[Cu(HL)Cl]\cdot CH_3OH$, the characteristic peak of enolic group disappeared, indicating that this oxygen participated in coordination. Meanwhile, the stretching vibrations of acylhydrazone C = O shifted approximately 30 $cm^{-1}$ towards the low wavenumber, indicating coordination also *via* acylhydrazone C = O [27]. Similar changes were found on the stretching vibrations of the acylhydrazone C = N which shifted approximately 35 $cm^{-1}$ towards low wavenumber, indicating the coordination of this nitrogen. The stretching vibrations of pyrazole ring C = N remained at 1512 $cm^{-1}$, suggesting that the ring nitrogen does not take part in coordination. In the far-IR region, new bands at 603 and 527 $cm^{-1}$ in the complexes are assigned to *v*(M-O) and *v*(M-N) [28] of stretching vibrations. These results could be ascertained by the crystal analysis as follows.

### 3.2. X-ray crystal structure of $[Cu(HL)Cl]\cdot CH_3OH$

X-ray structural analysis reveals that the mononuclear Cu(II) complex crystallized in the monoclinic system with $P2_1/c$ space group. The crystal structure of the complex with

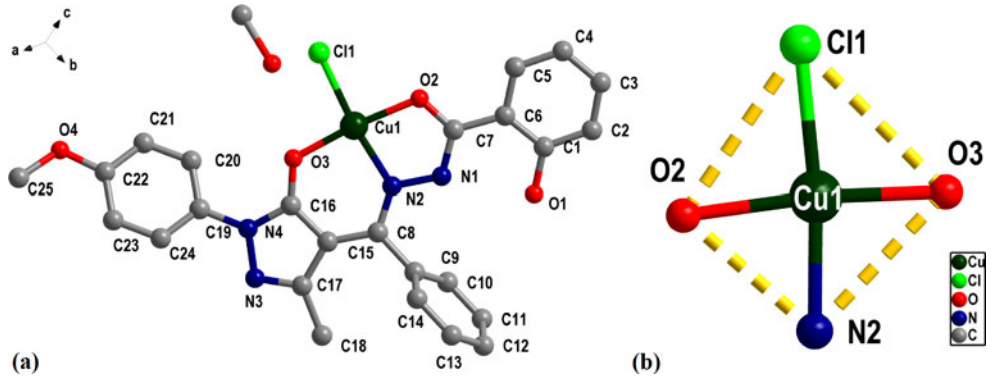


**Figure 2.** (a) View of the coordination environment of Cu1 center with thermal ellipsoids at 30% probability (all hydrogens have been omitted for clarity). (b) The coordination polyhedron of Cu1.

atomic numbering scheme is shown in Figure 2(a). Its asymmetric unit contains one crystallographically independent Cu(II) ion, one ligand anion $HL^-$ and one $Cl^-$ ion. Each Cu(II) atom is tetra-coordinated by atoms O2, O3 and N2 from one anionic ligand $HL^-$ and one $Cl^-$ ion (Cl1) to form a planar quadrilateral geometry as shown in Figure 2(b). The atoms O2, O5, N4 and Cl1 constitute the quadrilateral plane and the Cu(II) atom strays from the quadrilateral plane of 0.004 Å. The Cu–O2/O3 bond distances in quadrilateral plane are 1.950(3) Å/1.896(3) Å, the Cu–N2 bond distances are 1.954(3) Å, and the Cu–Cl1 bond distances are 2.221(3) Å. The angle of O2–Cu1–O3 is 174.26(11)° and the angle of Cl1–Cu1–N2 is 173.32(9)° which is slightly deviated from the theoretical value of 180°. Therefore, the local coordination geometry around the Cu(II) center can be described as a slightly distorted quadrilateral plane. Selected bond distances and angles for the Cu(II) complex are listed in Table S1 (Supplementary material). In addition, the bond lengths of O3–C16 (1.287(4) Å) and C15–C16 (1.412(5) Å) prove that oxygen O3 of the carbonyls participates in coordination by the enolic form, and their active hydrogen is replaced by the Cu(II) ion [29]. To test the purity of the bulk samples of the Cu(II) compound, the PXRD measurements was determined. As shown in Figure S3 (Supplementary material), the PXRD patterns of the bulk samples were similar to that of simulated, demonstrating the phase purity of the bulk samples of the Cu(II) compound.

To further analyze the crystal structure of the complex, significant hydrogen bonding interactions were found between the molecules. As shown in Figure 3(a), two mononuclear Cu(II) units are first connected by two crystalline methanol molecules in aid of hydrogen bonding where two crystalline methanol molecules serve as both donors and acceptors. The phenolic hydroxyl group of the ligand, the C–H on the benzene ring of the salicylhydrazide and pyrazolone acted as hydrogen bonding donor. The oxygen atom on the carbonyl group and the coordinated $Cl^-$ ion acted as hydrogen bond acceptor. Thus, a supramolecular macrocycle is formed through O1–H1···O5, O5–H5A···Cl1 and C10–H10···O2 hydrogen bonds between two Cu(II) molecules. With the help of the C14–H14···O3 hydrogen bond interaction, adjacent dimers can also be connected together, forming an infinite 1D chain along the a-axis, as shown in Figure 3(b). The distance of C14···O3 is 3.469 Å and the angle of C14–H14···O3 is 158.79°.

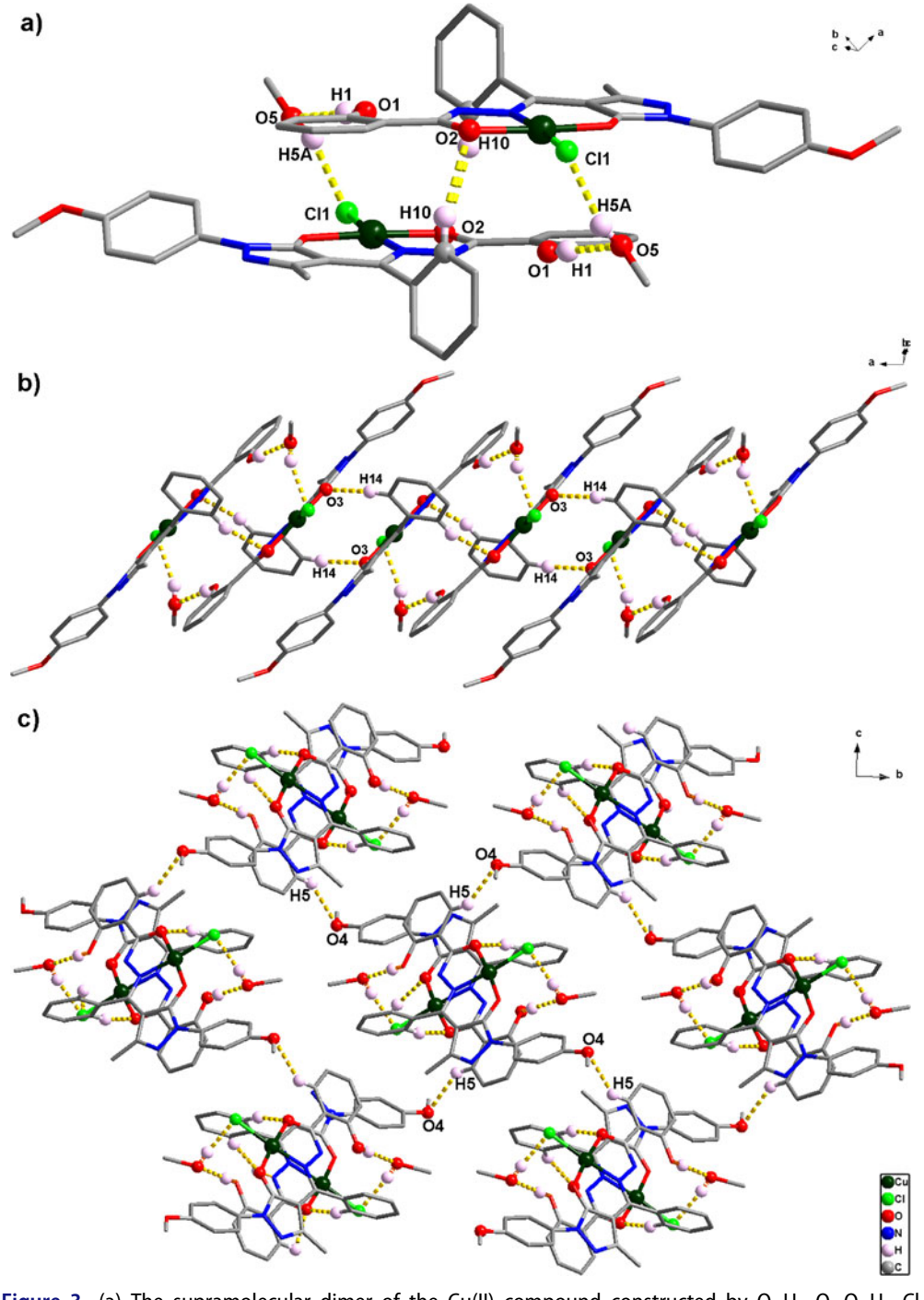


**Figure 3.** (a) The supramolecular dimer of the Cu(II) compound constructed by O–H···O, O–H···Cl and C–H···O hydrogen bonds; (b) The 1D supramolecular chain of the Cu(II) compound constructed by C–H···O hydrogen bonds; (c) The 3D supramolecular architecture constructed by C–H···O hydrogen bonds by two directions.

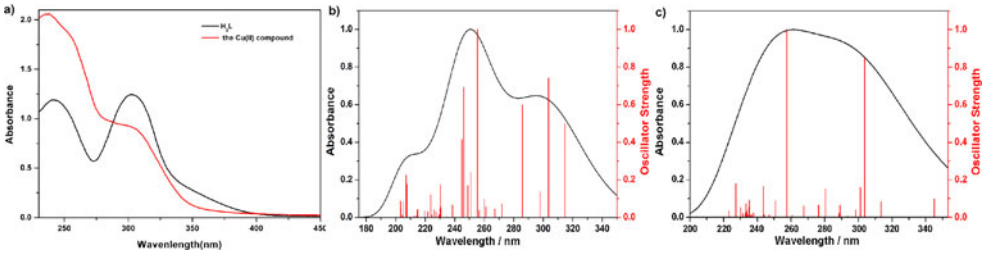


**Figure 4.** (a) UV–vis absorption spectra of $H_2L$ ($5.0 \times 10^{-5}$ M) and its Cu(II) compound ($5.0 \times 10^{-5}$ M) in $CH_3OH$ solution; (b) The simulated UV–vis absorption spectra of $H_2L$ in methanol with the oscillator strength of main excited states (strength $>$ 0.02) shown in red; (c) The simulated UV–Vis absorption spectra of the Cu(II) compound in methanol with the oscillator strength of main excited states (strength $>$ 0.02) shown in red.

Finally, the 1-D chain further forms an infinite 3D supramolecular framework by the interaction of C5–H5···O4 hydrogen bonds in two directions as shown Figure 3(c). The distance of C5···O4 is 3.430 Å and the angle of C5–H5···O4 is 147.38°. Selected hydrogen-bonding distances (Å) and angles (°) for Cu(II) complex are listed in Table S2 (Supplementary material), both within the ranges of those reported hydrogen bonds [30].

### 3.3. Absorption spectra study

In order to shed some light on the geometrical structure of the complex, the absorption spectra of $H_2L$ and $[Cu(HL)Cl]\cdot CH_3OH$ were recorded in methanol solution at room temperature (Figure 4(a)). The absorption spectrum of $H_2L$ consists of two bands at 242 and 302 nm, which are attributed to the $\pi \rightarrow \pi^*$ transitions of $H_2L$. The molar absorption coefficient value ($\varepsilon$) for $H_2L$ was calculated as $2.48 \times 10^4$ $M^{-1}cm^{-1}$, indicating that $H_2L$ has a strong ability to absorb light. A slight blue-shift was observed in the absorption spectrum after ligand coordination with copper, which is evidence of coordination of $H_2L$. To shed some light on the electronic spectra of $H_2L$ and its Cu(II) complex, TD-DFT calculations were performed on the optimized geometries of $H_2L$ and its Cu(II) compound in methanol with theoretical simulation of UV-vis absorption spectra of $H_2L$ and the Cu(II) complexes shown in Figures 4(b,c). The calculated vertical electronic excitation energy (eV) and oscillator strength (f) are summarized in Table 2.

The experimental absorption bands of the ligand and complex have been explained in aid of TD-DFT calculations. The intense bands of the ligand at 242 and 302 nm are intra-ligand charge-transfer (ILCT) characters in $H_2L$, while the corresponding theoretical bands are at 246 and 303 nm, in agreement with experimental results. As for the Cu(II) complex, the simulated peak at 246 nm and that of experiment at 236 nm is attributed to $\alpha$-HOMO–1 $\rightarrow$ $\alpha$-LUMO + 1 (53%) and $\beta$-HOMO–1 $\rightarrow$ $\beta$-LUMO + 2 transition (65%). Meanwhile, the simulated peak at 304 nm and the experimental one observed at 295 nm is corresponding to $\alpha$-HOMO–1 $\rightarrow$ $\alpha$-LUMO (49%) and $\beta$-HOMO–1 $\rightarrow$ $\beta$-LUMO transitions (63%). Clearly, the theoretical simulation results are in agreement with that of the experiment.

**Table 2.** TD-DFT Calculated electronic excitations of $H_2L$ and its Cu(II) compound in $CH_3OH$.

| Excitation (eV) | $\lambda_{ex}$ (nm) | Osc. strength (f) | Key transitions | Character | λexpt |
|---|---|---|---|---|---|
| $H_2L$ | | | | | |
| 4.0860 | 303.27 | 0.2681 | (56%) HOMO–1 → LUMO | $H_2L(\pi) \rightarrow H_2L(\pi^*)$ | 302 |
| 4.1649 | 297.64 | 0.0491 | (56%) HOMO–1 → LUMO | $H_2L(\pi) \rightarrow H_2L(\pi^*)$ | – |
| 5.0400 | 246.00 | 0.2501 | (58%) HOMO–1 → LUMO + 2 | $H_2L(\pi) \rightarrow H_2L(\pi^*)$ | 242 |
| 5.0664 | 244.15 | 0.1496 | (57%) HOMO–1 → LUMO + 3 | $H_2L(\pi) \rightarrow H_2L(\pi^*)$ | – |
| [Cu(HL)Cl]·$CH_3OH$ | | | | | |
| 2.9156 | 304.21 | 0.1649 | (49%) α-HOMO–1 → α-LUMO | $M(\pi) \rightarrow H_2L(\pi^*)$ | 295 |
| | | | (63%) β-HOMO–1 → β-LUMO | $M(\pi) \rightarrow H_2L(\pi^*)$ | |
| 2.9404 | 301.53 | 0.0311 | (24%) α-HOMO–2 → α-LUMO + 1 | $M(\pi) \rightarrow H_2L(\pi^*)$ | – |
| 3.4826 | 257.63 | 0.1944 | (50%) α-HOMO–4 → α-LUMO | $M(\pi) \rightarrow H_2L(\pi^*)$ | – |
| 3.6988 | 245.92 | 0.0322 | (35%) β-HOMO–3 → β-LUMO | $H_2L(\pi) \rightarrow H_2L(\pi^*)$ | 236 |
| | | | (53%) α-HOMO–1 → α-LUMO + 1 | $M(\pi) \rightarrow H_2L(\pi^*)$ | |
| | | | (65%) β-HOMO–1 → β-LUMO + 2 | $M(\pi) \rightarrow H_2L(\pi^*)$ | |

**Table 3.** Experimental and calculated bond distances (Å) in the Cu(II) compound.

| Bond lengths | Experimental | Calculated | Bond lengths | Experimental | Calculated |
|---|---|---|---|---|---|
| Cu1–O3 | 1.896 (2) | 1.90909 | Cu1–O2 | 1.950 (3) | 1.98949 |
| Cu1–N2 | 1.954 (3) | 1.98121 | Cu1–Cl1 | 2.2206 (11) | 2.26264 |

### *3.4. Theoretical calculations*

To better understand the electronic structure of the $H_2L$ and its Cu(II) complex, we performed density functional theory (DFT) calculations. The molecular geometry was optimized by the Gaussian 09 with the level of B3LYP. Nonmetal atoms were described by B3LYP/6-31G and metal atoms were treated by B3LYP/LANL2DZ basis sets. The optimized structures of $H_2L$ and the Cu(II) compound is displayed in Figure S4 (Supplementary material). As shown in Table 3, the optimized bond lengths for the Cu(II) complex are well replicated with the experimental one with minor deviations in bond distances in the range of 0.017–0.039 Å in Cu–O, 0.027 Å and 0.042 Å for Cu-N and Cu-Cl. The reason for the deviation is that the theoretical calculations were performed on an isolated molecule in gas phase whereas X-ray measurements being carried out in the solid state [31].

As shown in Figure 5(a), the calculated molecular orbital energies of the LUMO + 2, LUMO + 1, LUMO, HOMO, HOMO–1, and HOMO–2 for $H_2L$ are –0.625, –0.711, –1.229, –5.663, –6.065, and –6.133 eV, respectively. The energy gaps between HOMO–LUMO are 4.434 eV for $H_2L$. The calculated molecular α and β orbital energy of the HOMO and LUMO for the Cu(II) compound are –5.1930, –5.1911 and –2.2916, –2.3422 eV, respectively. The energy gaps between HOMO and LUMO are 2.9014 (α) and 2.8489 (β) for the Cu(II) compound as depicted in Figures 5(b,c). The plot of the highest occupied molecular orbitals (HOMOs) of the Cu(II) compound indicate that the HOMOs are comparatively less localized and reside mainly on the orbitals of the pyrazolone fragment. The LUMOs are delocalized and spread over the orbitals of the entire molecule.

As shown in Table 4, the HOMO–LUMO structures orbital energy occupying the boundary are all negative, testifying the chemical stability of the molecule [32, 33]. Compared with the experimental results, the calculated data are consistent with the UV-vis absorption spectra obtained from methanol solution. All

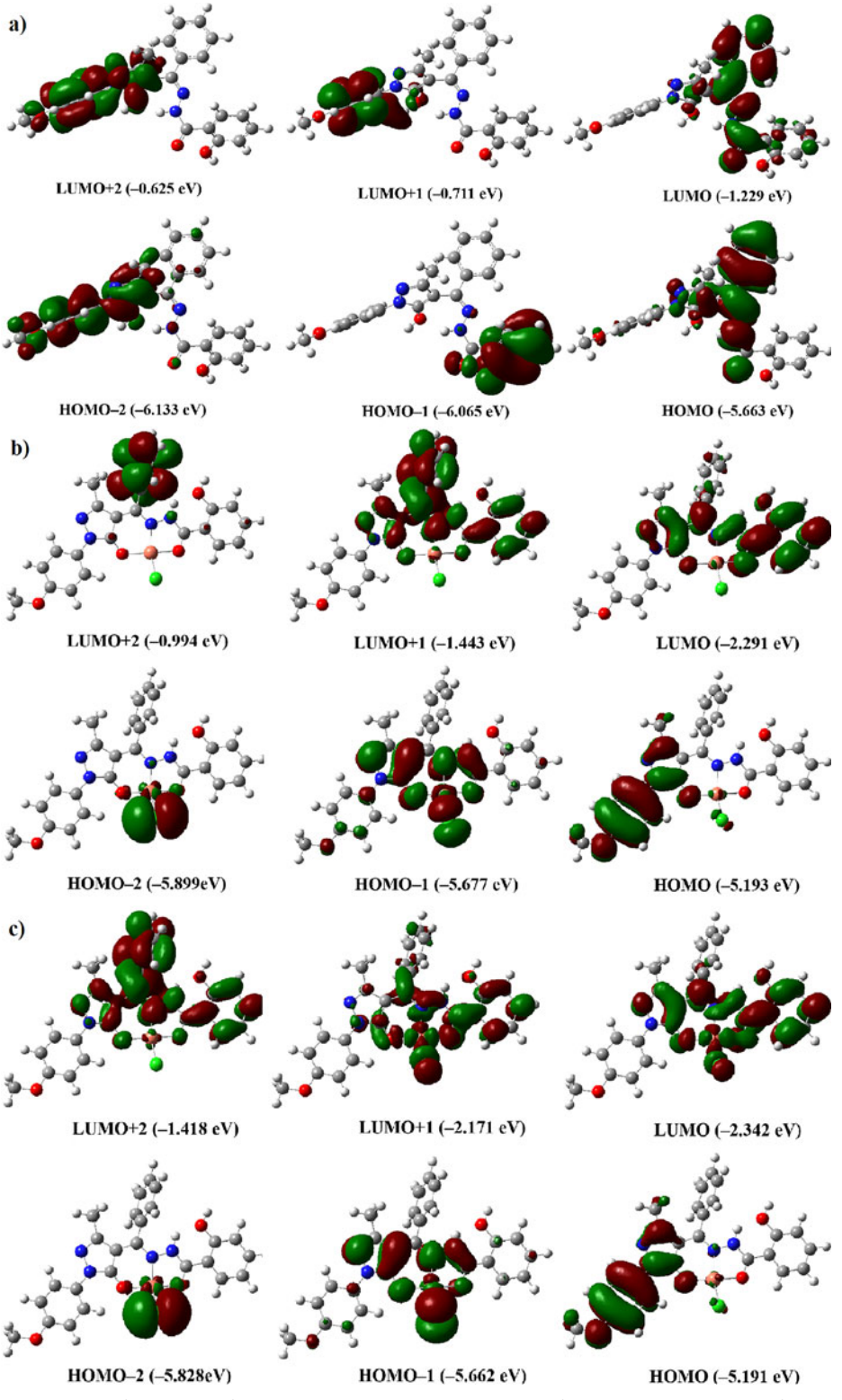


**Figure 5.** (a) Surface plots of some selected molecular orbitals of the ligand $H_2L$; (b) Surface plots of some selected molecular α-orbitals of the Cu(II) compound; (c) Surface plots of some selected molecular β-orbitals of the Cu(II) compound.

**Table 4.** Absorption spectra and HOMO–LUMO structures orbital energy of the Cu(II) compound.

| $\lambda_{edge}$ (nm) | $E^{opt}$ g [a](eV) | $E_{HOMO}$ (eV) | $E_{LUMO}$ (eV) | ΔEgap (eV) |
|---|---|---|---|---|
| 425 | 2.917 | −5.193 (α) | −2.291 (α) | 2.902 (α) |
| | | −5.191 (β) | −2.342 (β) | 2.849 (β) |

[a]$E^{opt}$g estimated from the UV–Vis absorption spectra.

these results indicate that the complex is stable and the DFT method with B3LYP/6–31G and B3LYP/LANL2DZ basis group used in the calculations is reasonable.

## 3.5. DNA-Binding experiments

### 3.5.1. Electronic absorption titration

Absorption spectrum titration is first utilized to characterize the binding mode and binding affinity of metal complexes with DNA by increasing the concentration of CT-DNA while the concentration of the test substance remained constant [34]. To obtain the absorption spectrum, the required amount of CT-DNA is added to the test solution as reference to eliminate the absorbance of CT-DNA itself. Each sample solution was scanned at a range of 190 nm to 500 nm and the mixture was balanced for 5 min before recording [35]. According to the absorption titration data, the following equation is used to obtain the DNA-binding constant [36]:

$$[DNA]/(\varepsilon_a-\varepsilon_f) = [DNA]/(\varepsilon_b-\varepsilon_f) + 1/K_b(\varepsilon_b-\varepsilon_f) \quad (1)$$

where [DNA] is the concentration of DNA in base pairs, $\varepsilon_a$ corresponds to the extinction coefficient observed ($A_{obsd}$/[M]), $\varepsilon_f$ corresponds to the extinction coefficient of the free compound, $\varepsilon_b$ is the extinction coefficient of the compound fully bounded to DNA, and $K_b$ is the intrinsic binding constant. The ratio of slope to intercept in the plot of [DNA]/($\varepsilon_a$ – $\varepsilon_f$) *versus* [DNA] gives the value of $K_b$.

The absorption spectra of $H_2L$ and the Cu(II) compound upon addition of CT-DNA are given in Figure 6. The intense absorption bands at 355 ∼ 380 nm observed in both $H_2L$ and its Cu(II) compound are attributed to intra ligand $\pi\rightarrow\pi^*$ transitions. Upon addition of CT-DNA, the absorption band of $H_2L$ shows a hypochromism of 4.86%. By contrast, the absorption band of the Cu(II) compound exhibits a hypochromism of 11.49% with a red-shift. Therefore, the Cu(II) compound is most likely to bind to DNA through an intercalative mode, because the hypochromic effect and red-shift of the UV absorption spectrum of metal complex was a result of an intercalating manner of DNA with metal compounds [37]. The binding constants $K_b$ for $H_2L$ and the Cu(II) compound has been determined from the plot of [DNA]/($\varepsilon_a$ – $\varepsilon_f$) *versus* [DNA] as shown in Figures 6(c,d). The $K_b$ of $H_2L$ and Cu(II) complex were $5.28 \times 10^3$ $M^{-1}$ ($R = 0.992$ for six points) and $2.83 \times 10^4$ $M^{-1}$ ($R = 0.995$ for nine points), respectively. The results show that the binding strength of the Cu(II) complex rises far above $H_2L$. Notably, the $K_b$ value is higher than that of the classical intercalator ethidium bromide (EB) *versus* CT-DNA [38], indicating that the binding strength between the Cu(II) complex and CT-DNA is very strong [39, 40].

Based on the experimental and theoretical results, the reasons for the strong binding of the Cu(II) compound to DNA was speculated to be electronic and spatial effects

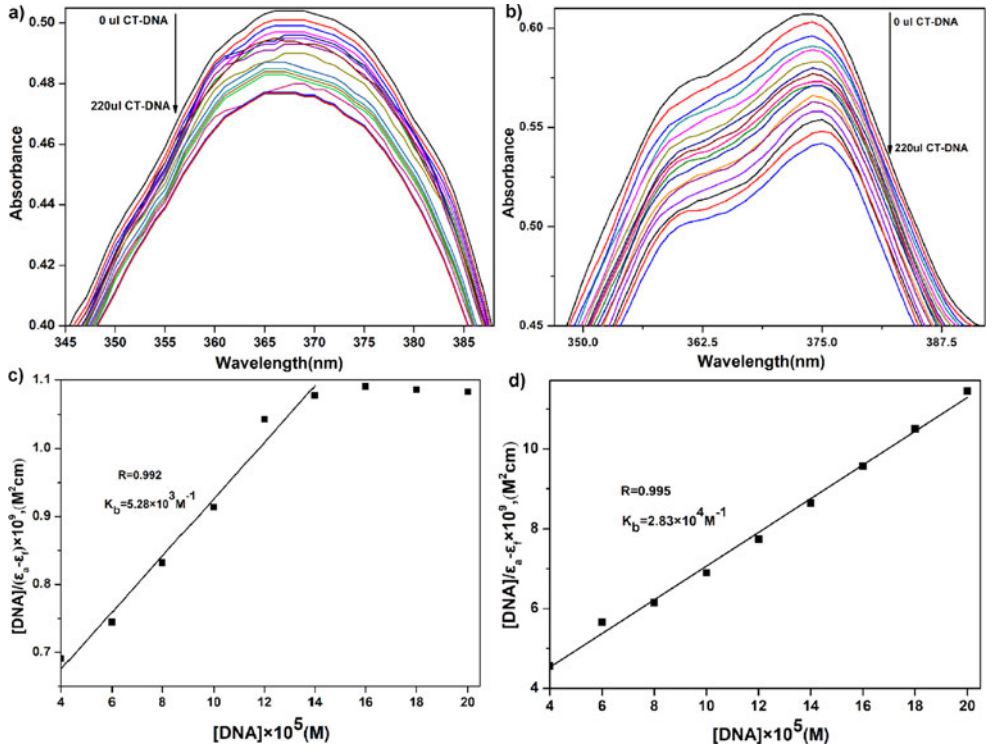


**Figure 6.** (a) Electronic spectra of $H_2L$ ($3 \times 10^{-3}$ M) in Tris-HCl buffer (pH = 7.2) upon addition of CT-DNA (0–220 μL, $2.5 \times 10^{-3}$ M) (arrow shows the emission intensity changes upon increasing DNA concentration); (b) Electronic spectra of the Cu(II) complex ($3 \times 10^{-3}$ M) in Tris-HCl buffer (pH = 7.2) upon addition of CT-DNA (0–220 μL, $2.5 \times 10^{-3}$ M) (arrow shows the emission intensity changes upon increasing DNA concentration); (c) Plots of [DNA]/($\varepsilon_a - \varepsilon_f$) *vs.* [DNA] for $H_2L$; d) Plots of [DNA]/($\varepsilon_a - \varepsilon_f$) *vs.* [DNA] for the Cu(II) complex.

caused by Cu(II)′s chelation as follows: (a) The increased co-planarity upon Cu(II) coordination may result in high affinity for DNA; (b) The reduced electron density on the ligand caused by the coordination of the central Cu(II) atom is conducive to embedding the DNA base pair.

### *3.5.2. EB-DNA fluorescence competition experiment*

In order to further study the binding properties of $H_2L$ and the Cu(II) complex with DNA, competitive binding experiment was carried out. Commonly, the fluorescence of EB is weak in solvent, but enhanced when embedded in DNA base pair. The addition of a second molecule competes with the EB for binding of DNA, allowing the fluorescence to quench, which demonstrates that the second molecule is embedded in the DNA base pair [41, 42]. Therefore, the binding degree between the second molecule and CT-DNA can be determined according to the degree of fluorescence quenching. For EB-DNA competition determination, 10 μL EB ($2.2 \times 10^{-3}$ M) solution and 10 μL DNA ($2.5 \times 10^{-3}$ M) stock solution were added to 2.5 mL Tris-HCl buffer solution (pH = 7.2), and the fluorescence spectra was determined upon excited at 520 nm. The

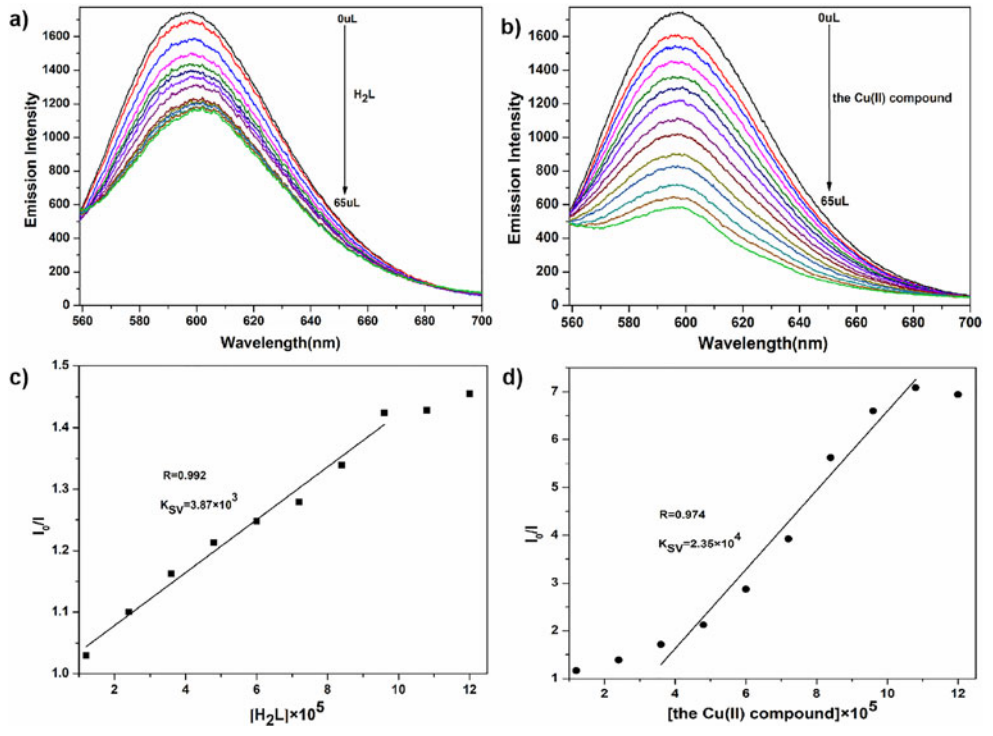


**Figure 7.** (a) Emission spectra of EB bound to CT-DNA excited at 520 nm in the presence of $H_2L$ ($3 \times 10^{-3}$ M); (b) Emission spectra of EB bound to CT-DNA in the presence of the Cu(II) compound ($3 \times 10^{-3}$ M); (c) Fluorescence quenching curves of EB bound to CT-DNA induced by $H_2L$; (d) Fluorescence quenching curves of EB bound to CT-DNA induced by the Cu(II) compound.

fluorescence quenching of EB-DNA bound induced by $H_2L$ and the Cu(II) complex are shown in Figures 7(a,b). With $H_2L$ and its Cu(II) compound gradually introduced into the EB-DNA solution (5 μL for each addition), respectively, the fluorescence intensities of EB-DNA centered at 598 nm obviously weakened under the same determination conditions. Based on the changes of fluorescence emission spectra, the influence of compounds added to EB-DNA complex solution was obtained [43, 44]. The spectra were analyzed according to the classical Stern-Volmer equation [45]:

$$I_0/I = \quad 1 \quad + K_{SV}[Q] \tag{2}$$

where $I_0$ and $I$ are the fluorescence intensities at 598 nm in the absence and presence of the quencher, respectively, $K_{SV}$ is the linear Stern-Volmer quenching constant, and [Q] is the concentration of the quencher.

The behavior of $H_2L$ and Cu(II) complex are in good agreement with the Stern-Volmer equation, which provides further evidence that the two compounds bind to DNA by embedding as depicted in Figures 7(c,d). The $K_{SV}$ values for $H_2L$ and the Cu(II) complex are $3.87 \times 10^3$ $M^{-1}$ ($R = 0.992$ for eight points) and $2.35 \times 10^4$ $M^{-1}$ ($R = 0.974$ for seven points), respectively. The higher quenching efficiency of the Cu(II) compound in contrast to that of $H_2L$ indicates that the Cu(II) compound has stronger DNA binding than $H_2L$ [46, 47], consistent with the absorption study results.

## 4. Conclusion

A new Cu(II) compound constructed by a new pyrazolone derivative was prepared and well characterized by IR, UV-vis and X-ray diffraction. Single-crystal X-ray analysis reveals that the Cu(II) compound presented herein exhibits interesting supramolecular characteristics and a novel 3D supramolecular architecture was resulted due to the appropriate synergy of multiple intermolecular hydrogen bonds. Furthermore, TD-DFT have been performed on optimized geometries for a better understanding of the electronic transitions in the UV-vis spectra of $H_2L$ and the Cu(II) complex. Electronic absorption titration and EB-DNA competition experiment indicate that the Cu(II) complex are combined with DNA in an embedded manner and has a strong affinity for binding. This study clearly shows the effect of copper complexes on DNA and provides a foundation for further research and development of new metal anticancer drugs.

## Disclosure statement

No potential conflict of interest was reported by the authors.

## Funding

This work was supported by the National Natural Science Foundation of China (Grant 21661019).

## References

[1] C. Hemmert, M. Piti, M. Renz, H. Gornitzka, S. Soulet, B. Meunier. *J. Biol. Inorg. Chem.*, **6**, 14 (2001).
[2] M.M. Aleksić, V. Kapetanović. *Acta Chim. Slov.*, **61**, 555 (2014).
[3] G. Zuber, J.C. Quada, S.M. Hecht. *J. Am. Chem. Soc.*, **120**, 9368 (1998).
[4] K.J. Barnham, M.I. Djuran, P. d S. Murdoch, J.D. Ranford, P.J. Sadler. *Inorg. Chem.*, **35**, 1065 (1996).
[5] (a) B.J. Pages, D.L. Ang, E.P. Wright, J.R. Aldrich-Wright. *Dalton Trans.*, **44**, 3505 (2015). (b) R. Galindo-Murillo, J.C. García-Ramos, L. Ruiz-Azuara, T.E. Cheatham, F. Cortés-Guzmán. *Nucleic Acids Res.*, **43**, 5364 (2015). (c) G. Palermo, A. Magistrato, T. Riedel, T. Erlach, C.A. Davey, P.J. Dyson, U. Rothlisberger. *ChemMedChem*, **11**, 1199 (2016).
[6] (a) S. Niroomand, M. Khorasani-Motlagh, M. Noroozifar, A. Moodi. *J. Photochem. Photobiol. B*, **117**, 132 (2012). (b) H. Wu, Y. Bai, Y. Zhang, Z. Li, M. Wu, C. Chen, J. Zhang. *J. Coord. Chem.*, **67**, 3054 (2014). (c) H. Wu, Y. Zhang, C. Chen, J. Zhang, Y. Bai, F. Shi, X. Wang. *New J. Chem.*, **38**, 3688 (2014). (d) H. Wu, J. Zhang, C. Chen, H. Zhang, H. Peng, F. Wang, Z. Yang. *New J. Chem.*, **39**, 7172 (2015). (e) C. Chen, J. Zhang, Y. Zhang, Z. Yang, H. Wu, G. Pan, Y. Bai. *J. Coord. Chem.*, **68**, 1054 (2015). (f) H. Zhang, Y. Xu, H. Wu, S.O. Aderinto, X. Fan. *RSC Adv.*, **6**, 83697 (2016). (g) S. Mao, K. Shen, X. Shi, Y. Xu, H. Wu. *J. Coord. Chem.*, **70**, 3677 (2017). (h) J. Haribabu, M.M. Tamizh, C. Balachandran, Y. Arun, N.S.P. Bhuvanesh, A. Endo, R. Karvembu. *New J. Chem.*, **42**, 10818 (2018).
[7] J. Shao, W.G. Bao, H. Tian, B. Li, X.F. Zhao, X. Qiao, J.Y. Xu. *Dalton Trans.*, **43**, 1663 (2014).
[8] F. Samari, B. Hemmateenejad, M. Shamsipur, M. Rashidi, H. Samouei. *Inorg. Chem.*, **51**, 3454 (2012).

[9] F. Dimiza, C.P. Raptopoulou, V. Psycharis, A. Papadopoulos, G. Psomas. *New J. Chem.*, **42**, 16666 (2018).
[10] M. Zampakou, S. Balala, F. Perdih, S. Kalogiannis, I. Turel, G. Psomas. *RSC Adv.*, **5**, 11861 (2015).
[11] D. Inci, R. Aydin, Ö. Vatan, O. Sahin, N. Çinkiliç. *New J. Chem.*, **43**, 4681 (2019).
[12] R.P. Sharma, S. Kumar, P. Venugopalan, V. Ferretti, A. Tarushi, G. Psomas, M. Witwicki. *RSC Adv.*, **6**, 88546 (2016).
[13] H. Wu, H. Wang, X. Wang, G. Pan, F. Shi, Y. Zhang, Y. Bai, J. Kong. *New J. Chem.*, **38**, 1052 (2014).
[14] J. Joseph, K. Nagashri, G.B. Janaki. *Eur. J. Med. Chem.*, **49**, 151 (2012).
[15] H.L. Wu, Z.H. Yang, F. Wang, H.P. Peng, H. Zhang, C.P. Wang, K.T. Wang. *J. Photochem. Photobiol. B*, **148**, 252 (2015).
[16] J. Joseph, K. Nagashri, A. Suman. *J. Photochem. Photobiol. B*, **162**, 125 (2016).
[17] G. Mariappan, B.P. Saha, L. Sutharson, A. Singh, S. Garg, L. Pandey, D. Kumar. *Saudi Pharm. J.*, **19**, 115 (2011).
[18] X.M. Peng, G.X. Cai, C.H. Zhou. *Curr. Top. Med. Chem.*, **13**, 1963 (2013).
[19] J.S. Casas, M.S. Garcia-Tasende, A. Sanchez, J. Sordo, A. Touceda. *Coord. Chem. Rev.*, **251**, 1561 (2007).
[20] X.-Q. Song, Y.-Q. Peng, G.Q. Cheng, X.-R. Wang, P.-P. Liu, W.-Y. Xu. *Inorg. Chim. Acta*, **427**, 13 (2015).
[21] S.B. Desai, P.B. Desai, K.R. Desai. *Heterocycl. Commun.*, **7**, 83 (2001).
[22] S. Satyanaryana, J.C. Dabrowiak, J.B. Chaires. *Biochem. J.*, **32**, 2573 (1993).
[23] J. Marmur. *J. Mol. Biol.*, **3**, 208 (1961).
[24] *Smart & Saint*, Bruker AXS Inc., Madison, WI (2014).
[25] G.M. Sheldrick. *Shelxl-2014*, University of Gottingen, Gottingen, Germany (2014).
[26] K. Brandenburg. Diamond (version 3.2), crystal and molecular structure visualization. In *Crystal Impact, Gbr*, K. Brandenburg, H. Putz (Eds.), Bonn, Germany (2009).
[27] (a) I.A. Patel, B.T. Thaker, P.B. Thaker. *Indian J. Chem.*, **37**, 429 (1998). (b) I.A. Patel, B.T. Thaker. *Indian J. Chem.*, **38**, 427 (1999).
[28] B.M. Mohapatta, V. Chakravortty, K.C. Das. *Polyhedron*, **8**, 1509 (1989).
[29] P. Cui, Z. Chen, D.L. Gao, B. Zhao, W. Shi, P. Cheng. *Cryst. Growth Des.*, **10**, 4370 (2010).
[30] (a) X.Q. Song, W.S. Liu, W. Dou, Y.W. Wang, J.R. Zheng, Z.P. Zang. *Eur. J. Inorg. Chem.*, **11**, 1901 (2008). (b) X.Q. Song, L. Wang, M.M. Zhao, G.Q. Cheng, X.R. Wang, Y.P. Qiao. *Inorg. Chim. Acta*, **402**, 156 (2013). (c) X.Q. Song, D.Y. Xing, Y.K. Lei, M.M. Zhao, G.Q. Cheng, X.R. Wang, Y.P. Qiao. *Inorg. Chim. Acta*, **404**, 113 (2013).
[31] L.Q. Chai, L.J. Tang, L.C. Chen, J.J. Huang. *Polyhedron*, **122**, 228 (2017).
[32] R.N. Patel, Y. Singh, Y.P. Singh, R.J. Butcher. *J. Coord. Chem.*, **15**, 1 (2016).
[33] L.Q. Chai, Q. Hu, K.Y. Zhang, L. Zhou, J.J. Huang. *J. Lumin.*, **203**, 234 (2018).
[34] C.Y. Chen, J.W. Zhang, Y.H. Zhang, Z.H. Yang, H.L. Wu, G.L. Pan, Y.C. Bai. *J. Coord. Chem.*, **68**, 1054 (2015).
[35] H.L. Wu, J.W. Zhang, C.Y. Chen, H. Zhang, H.P. Peng, F. Wang, Z.H. Yang. *New J. Chem.* , **39**, 7172 (2015).
[36] A.M. Pyle, J.P. Rehmann, R. Meshoyrer, C.V. Kumar, N.J. Turro, J.K. Barton. *J. Am. Chem. Soc.*, **111**, 3051 (1989).
[37] M. Baldini, M. Belicchi-Ferrari, F. Bisceglie, P.P. Dall'Aglio, G. Pelosi, S. Pinelli, P. Tarasconi. *Inorg. Chem.*, **43**, 7170 (2004).
[38] A. Dimitrakopoulou, C. Dendrinou-Samara, A.A. Pantazaki, M. Alexiou, E. Nordlander, D.P. Kessissoglou. *J. Inorg. Biochem.*, **102**, 618 (2008).
[39] H.L. Wu, T. Sun, B. Liu, K. Li, F. Jia, J.K. Yuan, F. Kou. *Synth. React. Inorg. Met.-Org. Nano-Met. Chem.*, **41**, 577 (2011).
[40] H.L. Wu, Y.H. Zhang, Y.C. Bai, X.L. Wang, J. Kong, F.R. Shi. *Synth. React. Inorg. Met.-Org. Nano-Met. Chem.*, **45**, 1474 (2015).
[41] A. Wolf, G.H. Shimer, T. Meehan. *Biochemistry*, **26**, 6392 (1987).

[42] B.C. Baguley, M.L. Bret. *Biochemistry*, **23**, 937 (1984).
[43] M. Tümer, H. Köksal, M.K. Sener, S. Serin. *Transit. Met. Chem.*, **24**, 414 (1999).
[44] E.N. Chygorin, O.V. Nesterova, J.A. Rusanova, V.N. Kokozay, V.V. Bon, R. Boca, A. Ozarowski. *Inorg. Chem.*, **51**, 386 (2012).
[45] J.R. Lakowicz, G. Weber. *Biochemistry*, **12**, 4161 (1973).
[46] H.L. Wu, F. Wang, F.R. Shi, Z.H. Yang, H. Zhang, H.P. Peng. *Transit. Met. Chem.*, **40**, 555 (2015).
[47] H.L. Wu, G.L. Pan, Y.C. Bai, H. Wang, J. Kong, F.R. Shi, Y.H. Zhang, X.L. Wang. *Res. Chem. Intermed.*, **41**, 3375 (2015).